Available online at www.sciencedirect.com

ScienceDirect

Procedia Manufacturing 48 (2020) 781–789

Procedia MANUFACTURING

www.elsevier.com/locate/procedia

48th SME North American Manufacturing Research Conference, NAMRC 48 (Cancelled due to COVID-19)

Impact of Surface Roughness and Porosity on Lattice Structures Fabricated by Additive Manufacturing- A Computational Study

Panwei Jiang[a], Mustafa Rifat[b], Saurabh Basu[b,*]

[a]*Department of Materials Science and Engineering, The Pennsylvania State University, University Park, PA 16802, USA*
[b]*Harold and Inge Marcus Department of Industrial and Manufacturing Engineering, The Pennsylvania State University, University Park, PA 16802, USA*

Abstract

Research in this article presents a computational analysis of effects of defects in 2.5D lattice structures fabricated by Additive Manufacturing (AM). Components resulting from AM often suffer from rough surfaces and porosity defects. This complicates their response which must be understood for their service deployment. The core of the methodology used in this research is a workflow for generating various defects such as surface roughness and porosity analogous to those that naturally result from AM-fabricated lattices. Surface roughness is introduced by either discretizing a sinusoidal function or fitting experimental roughness data by Fourier Transforms. Porosity defects are implemented by drawing ellipses with assigned center position, radius and aspect ratio. A plane stress Finite Element Method (FEM) model is used under a uniform displacement boundary condition. Stress-strain and stiffness of the lattices are characterized as a function of the implanted defect. This methodology enables characterization of the effect of: (i) surface roughness, (ii) porosity defect density, (iii) porosity defect size, and (iv) algorithms with which random defects can be generated in simulated specimens. Effectiveness of this workflow also provides an efficient way to generate an adequate data pool for future machine learning and other data processing work.

Keywords: additive manufacturing; lattice structure; surface roughness; porosity defects; finite element method

1. Introduction

Additive manufacturing (AM) has become a popular materials processing method for rapidly fabricating complex tailor-made geometries [1, 2]. Stainless steels, nickel and titanium alloys are common choices for fabricating parts with AM due to their utility in high-performance applications[3, 4, 5, 6, 7]. Common AM configurations for fabricating these components include methods like electron beam melting (EBM) and selective laser melting (SLM) [8, 9].

Control over these manufacturing variables, e.g. material and process, make AM ideally suited for fabricating lattice structures for high performance applications in different sectors. These structures refer to topologically ordered and open cell lattice-like configurations such as body centered cubic unit cell with vertical struts (BCCZ), face and body centered cubic unit cell with vertical struts (FBCCZ), face and body centered cubic unit cell with vertical and horizontal struts (FBCCXYZ) [10, 11]. Interest in lattice structures for various applications arises primarily from their superior strength to weight ratio. This characteristic may also simultaneously benefit extraneous functions, e.g. ventilation assisted mitigation of corrosion [12, 13] and acoustic properties. Research on mechanical behavior of lattice structures has looked at their mechanical properties and characteristics under different load conditions such as compression, shear or blast loading [14, 15, 16, 17, 18].

Unfortunately, AM-fabricated parts normally suffer from poor surface roughness and porosity defects. These imperfections naturally arise during the AM process [19, 20] and adversely affect resulting mechanical, e.g. elastic [21] and plastic [22] deformation behavior. Hence, these defects must be mitigated to achieve ideal performance from lattice structures. However, efficacy of approaches for their mitigation, e.g. post-processing and hot iso-static pressing decreases as the complexity of lattice structure geometry increases. In this regard, recent research efforts have looked at approaches to encapsulate effects arising out of tolerable defects in the design of lattice structures. From the context of finishing lattice structures to make their defects tolerable, the question naturally arises, what is tolerable or good enough.

* Corresponding author.
E-mail address: sxb514@psu.edu (Saurabh Basu).

10.1016/j.promfg.2020.05.114

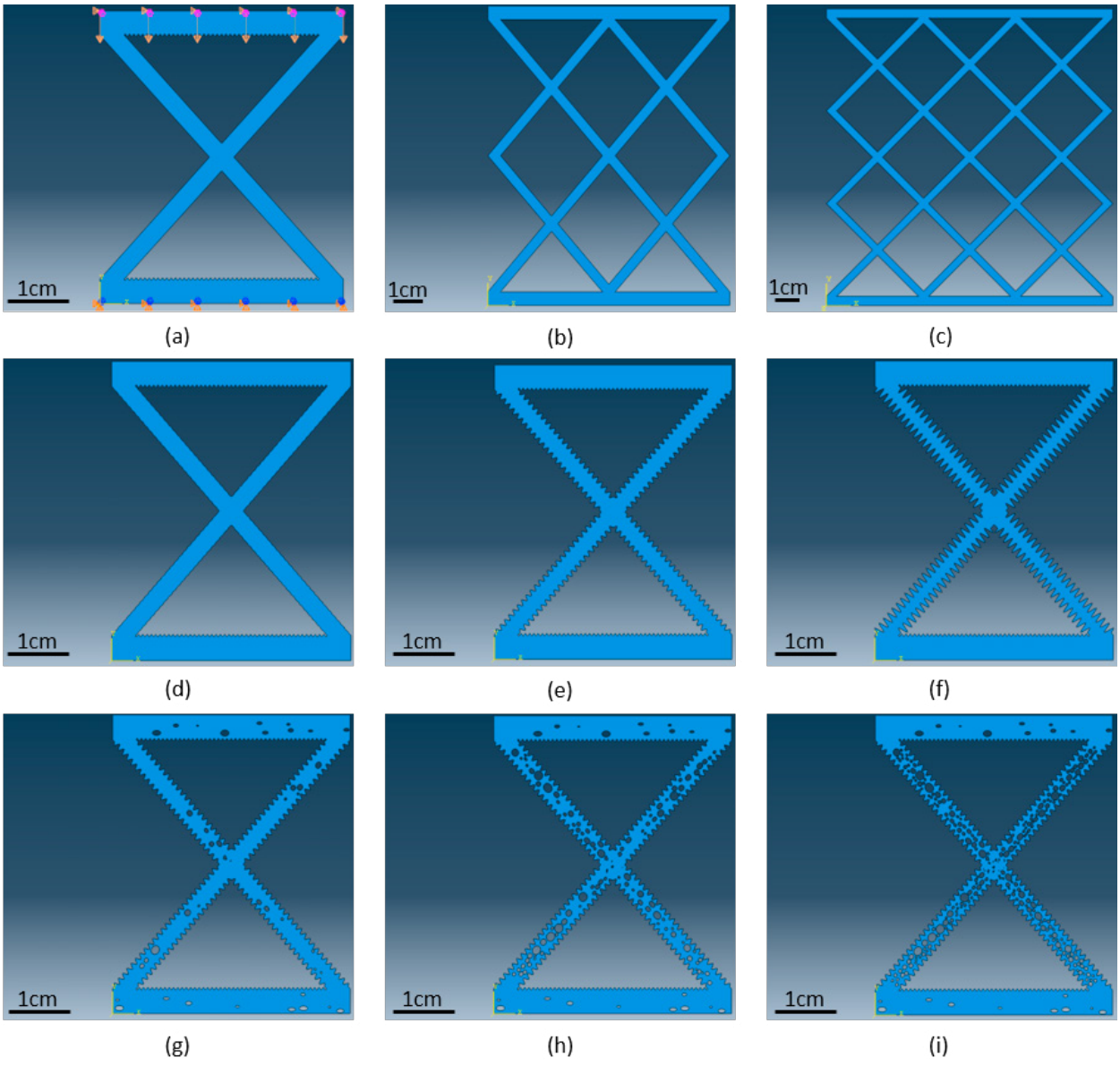

Fig. 1. Lattice structures with smooth surface and with (a) 1×1 layer; (b) 2×2layers; and (c) 3×3 layers; Lattice structure with 1×1 layer and with (d) $Ra = 23\mu m$; (e) $Ra = 231\mu m$; and (f) $Ra = 464\mu m$; Lattice structure with 1×1 layer, $Ra = 23\mu m$
, 10 pores on each shell and (g) 10 pores on each strut; (h) 50 pores on each strut; and (i) 120 pores on each strut

Computational methods provide an effective approach to predict effects of defects in lattice structures that result from AM. This methodology involves planting of defects featuring a statistically similar makeup as those observed in real lattice structures in their computational counterparts. This is followed by application of displacement or force boundary conditions to the computational structures and characterization of their response. The same methodology is also effective in simulating the material state that results directly from the AM characterized by its residual stress field [23].

Due to high computational requirements when deformation of lattice arrays comprising a large number of repeat units is simulated, the aforementioned approach is adapted with mechanically equivalent members [24, 30, 31] that feature statistically similar defects while reducing the number of elements required for simulation. Although this approach accelerates the simulation process, the methodology ignores volume porosity defects that are common place in components resulting from AM, focusing primarily on effect of surface roughness. Studies that have attempted to simulate effects of porosity defects

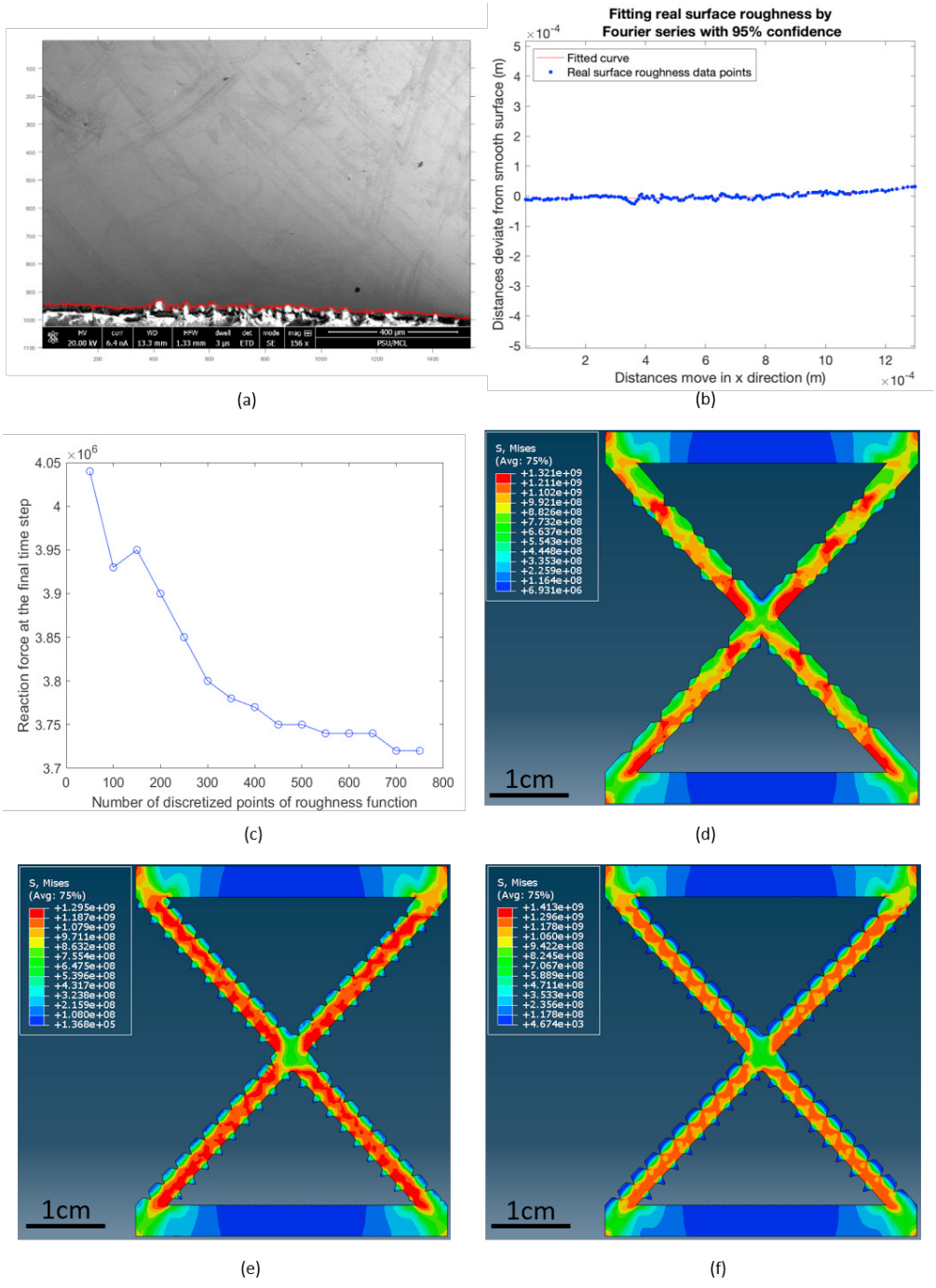

Fig. 2. (a) SEM image of real surface from an AM-fabricated part; (b) Fitting curve of Fourier series; (c) Effect of points number in roughness function; (d) Stress field for 50 points discretizing roughness function; (e) Stress field for 200 points discretizing roughness function; (f) Stress field for 750 points discretizing roughness function

on mechanical behavior by full field finite element modeling (FEM) have however suggested that even large pores do not affect the mechanical behavior of lattice structures significantly [32].

In the present study, a FEM based computational framework is created to understand the effects of surface roughness and porosity on mechanical response of 2.5D (e.g. plane-stress) lattice structures. Effects of roughness and porosity area fraction are normalized with respect to strut thickness and analyzed with respect to the number of repeat units in the structure. Novel contributions of the work include delineation of methodology for creating numerical frameworks for testing of various stochastic distributions of defects in various structures. Herein, artefacts arising from pseudo-randomness of stochastic defects generated in computer during their numerical implantation are discussed. Utility of this methodology is demonstrated in parametric delineation of effects of defects on various lattices that feature different designs and defect structures.

2. Finite Element Model

2.1. Geometry of Lattice Structure and Boundary Conditions

A script was created to generate 2.5D BCC lattice structures via the Python interface of Abaqus. Four parameters are needed to generate a lattice structure: (i) distance d between the top and bottom horizontal shell struts, (ii) length l of horizontal strut walls, (iii) thickness t_{shell} of horizontal struts, and (iv) thickness t_{strut} of oblique struts. The dimensions of a 1-layer lattice structure used in this work are listed in table 1. The angle θ between oblique struts and shells are naturally determined by this parameterization as $\theta = \arctan(\frac{d}{l-t_{strut}})$. Multi-layer lattice structures were created by repeating the unit cell in horizontal and vertical directions as listed in table 2 and shown in Figs. 1a-1c. For understanding the effect of roughness and porosity on mechanical behavior, these lattice structures were implanted with defects as described in sections 2.3 and 2.4. These defective structures are summarized in Figs. 1d-1i.

The elastic and yield behavior of these structures was evaluated during their compression for which the bottom surface was held stationary and the top surface was descended at speed $v = 4.8 \times 10^{-4}\ m/s$ for 1 second to produce a displacement of $vt = 4.8 \times 10^{-4}\ m$ in all specimens. These boundary conditions resulted in a true compressive strain and strain rate of $\epsilon \sim 0.01$ and $\dot{\epsilon} = 0.01\ s^{-1}$. Dynamic elastic effects were ignored.

Table 1. Dimension of a unit cell of a BCC type 2D shell lattice structure.

$d\ (m)$	$l\ (m)$	$t_{shell}\ (m)$	$t_{strut}\ (m)$
0.04	0.04	0.004	0.004

Table 2. Number of repeat units in multi-layer lattice structures

	1 by 1	2 by 2	3 by 3
number of struts in the horizontal	2	4	6
number of struts in the vertical	2	4	6
Total number of struts	2	8	18

2.2. Material

Two material attributes of Inconel 718 were implemented in the FEM framework:(i) Isotropic elasticity, and, (ii) Johnson Cook (JC) plasticity. The JC model is specified by Eqn.1 [27]. The material properties of Inconel 718 used in this research are listed in table 3 [25, 26, 27]. Simulations were executed in plane stress mode. Plane stress thickness was not specified and hence the unit of reaction force in the output of the FEM framework was (N/m). Three-node linear plane stress element CPS3 and four-node bilinear reduced integration plane stress element CPS4R were used. Stress fields and reaction forces resulting from the imposed displacement boundary conditions were characterized. The choice of plane stress deformation mode in the present work via 2.5D structures results in simplification of analysis and may not capture insights pertinent to the behavior of complex 3D structures. However, these simple 2.5D structures were intentionally chosen in the present exploratory analysis to eliminate variables, i.e. more complex stress states that exist in 3D structures. This was done for testing the robustness of this computational methodology in delineating effects of roughness and porosity defects in simplified, e.g. 2.5D plane stress settings. Efforts are underway to address analogous questions in 3D structures.

$$\overline{\sigma} = [A + B(\overline{\epsilon}^{pl})^n][1 + Cln(\frac{\dot{\overline{\epsilon}}^{pl}}{\dot{\epsilon}_0})][1 - (\frac{T - T_{room}}{T_{melt} - T_{room}})^m] \quad (1)$$

Table 3. Materials parameters used in FEM model [25][26].

Materials		Inconel 718
Density (kg/m^3)		8821
Young's modulus (Pa)		2.12×10^{11}
Poisson's ratio		0.294
Johnson-Cook parameters	A (Pa)	1.241×10^9
	B (Pa)	6.22×10^8
	n	0.6522
	m	1.3
	$T_m(^\circ C)$	1255
	$T_r(^\circ C)$	25
	C	0.0134
	$\dot{\epsilon}$	1

2.3. Surface roughness

In order to assess the effect of real roughness textures that originate from AM, Inconel 718 specimens were printed using direct metal laser sintering in an EOS M 280 machine. The laser spot diameter was set at 87.5 μm and the layer thickness was set at 40 μm. The laser power level was preset at 285 W. The as-received surface of the specimen was characterized by exposing it's cross section by electric discharge machining. Subsequently, the cross section was imaged using scanning electron microscopy (SEM) as seen in Fig. 2a. A MATLAB script was used to extract discrete data points from this cross section. Fourier series was used to fit data points as given in Eq. 2 [28],

and shown in Fig. 2b. In this manner, a real surface roughness profiles was quantified as a numerical roughness pattern that was then processed to be implanted onto the simulated specimen using the Python interface of Abaqus. The Fourier series pattern was repeated to cover the length of the specimen.

$$y = a_0 + \sum_{k=1}^{N} a_k \cos\left(\frac{2\pi k x}{\lambda}\right) + b_k \sin\left(\frac{2\pi k x}{\lambda}\right) \quad (2)$$

Unfortunately, this approach of assessing effects of surface roughness is computationally expensive due to a minimum density of surface nodes required to adequately represent texture. For instance, a larger node density results in a larger number of elements in the simulation thus slowing it down. Clearly, inclusion of smaller wavelengths in the Fourier series for representation of textures dictates greater required node density by the Nyquist criterion and hence, will result in a slower simulation. This is important from the context of optimization as the same surface texture may be represented by a larger node density to greater accuracy, but this endeavor may only provide diminishing additional insights. To assess these effects, different number of points were used to discretize the same roughness function (Fig.2c-f). Their reaction force at the final time step upon application of the boundary conditions described in section 2.1 was extracted from the FEM model and compared.

In addition to surface roughness obtained from real specimen, the effect of ideal, e.g. sinusoidal roughness on mechanics was also analyzed. Sinusoidal function $y = a\sin(\frac{2\pi}{\lambda}x)$ was used to generate roughness on struts, where wavelength λ is set to $1.076mm$. The amplitudes a and their corresponding roughnesses R_a that were tested include parameters $(a, R_a) = (4\times10^{-5}, 23\mu m), (4\times10^{-4}, 231\mu m), (8\times10^{-4}, 464\mu m)$. Here, parameter R_a refers to $R_a = \frac{1}{n}\sum_{i=1}^{n} |\, y_i \,|$, where y is the deviation of the assessed profile. The effect of these roughnesses was assessed by imposing the same displacement boundary conditions as described in section 2.1.

2.4. Porosity Defects

The effect of random porosity defects was assessed in terms of: (i) density, (ii) size, and (iii) algorithm for generation of random number that enables implantation of random pores. These numerical specimens were generated as described in sections 2.4.1, 2.4.2 and 2.4.3 and subject to the same boundary conditions as described in section 2.1 to assess their defects. Random number seeds 4&10 were used for the left and right leaning struts unless specified otherwise.

2.4.1. Density

A preset number $n = 0 - 120$ of porosity defects was implanted in random locations on a unit lattice structure specimens featuring a surface roughness $R_a = 231\mu m$. The defects were generated as circles with radii sampled from uniform distributions whose range was set in $(0.05t_{strut}, 0.2t_{strut})$. Subsequently, these circles were deformed and made elliptical by stretching one axis to provide them with an aspect ratio that was sampled from a uniform distribution whose range was set in $(0.7, 1)$.

2.4.2. Size

Porosity defects amounting to 2.72% area fraction were implanted in the simulated unit lattice structure specimens at random locations. The shapes of these defects were elliptical in this suite of plane stress simulations. In order to test the effect of size of porosity defects, these ellipses were generated by sampling radii of circles from uniform distribution whose ranges were set as $(0.05t_{strut}, 0.2t_{strut}), (0.1t_{strut}, 0.2t_{strut}), (0.15t_{strut}, 0.3t_{strut}), (0.2t, 0.35t_{strut})$, where t_{strut} is the strut thickness. Subsequently, aspect ratios were sampled from uniform distribution whose range was set between $(0.7, 1)$ to deform these circles into ellipses. Finally, the struts were implanted with a default surface roughness $R_a = 231\mu m$, where t_{strut} is the thickness of the parent strut. In these simulations, the porosity on the top and bottom shell were also set at 2.72% by default.

2.4.3. Random Number Generation Algorithm

Random numbers were generated for this research by function PRNG in python that needs specification of a random number seed. The supporting inbuilt algorithm is often used by other numerical computing programs that also take a seed as input for generating random numbers. This renders a pseudo randomness to the list of number generated, making them completely reproducible as long as the same seed is specified again. This implies that results of these simulations are highly influenced by the chosen seed. This effect is analyzed by generating random numbers with various seeds for creating porosity defects and assessing variations in their behavior using the same boundary conditions as described in section 2.1. In order to minimize the effect of pseudo randomness, position and dimensions of elliptical porosity defects on top and bottom shells were kept constant, wherein area fraction of defects was maintained at 2.72%. Further, the seed of PRNG was set at 1 for the top shell and 2 for the bottom shell. The instance with seed 4 for the strut inclined towards top left, and 10 for the strut inclined to top right was used as reference.

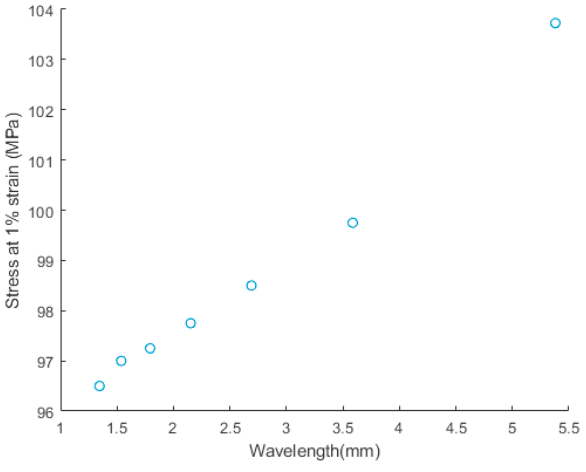

Fig. 3. Effect of waviness on response of 1×1 lattice structures featuring a roughness $R_a = 231\mu m$.

3. Results and Discussion

3.1. Effect of Surface Roughness on Mechanics of Lattices

3.1.1. Effect of resolution of discretization

The effect of resolution for discretization of the real surface roughness was evaluated by simulating deformation of these lattice structures using the conditions described in section 2.1. The reaction stress along with stress fields at the end of the deformation for various levels of discretizaiton are shown in Figs. 2c-2f. Figure 2c shows that a higher discretization level creates a smaller reaction stress. This effect arises from a competition between roughness and waviness. Roughness of a surface refers to prominent wave components that feature smaller wavelengths, whereas waviness generally refers to wave components with larger wavelengths. As long as the waviness of a component surface does not compromise its structural response by activating unstable deformation modes (e.g. buckling), a wavy surface results is greater stiffness compared to a rough surface. Herein, discretization of the real roughness profiles with coarser resolution naturally provides a low pass filter effect due to which, the effect of smaller wavelength roughness features are eliminated. This hypothesis was further evaluated by testing the response of structures featuring sine waves with amplitudes and roughness $(a, R_a) = (4 \times 10^{-4}, 231\mu m)$, and wavelengths $1.1\ mm < \lambda < 5.5\ mm$. The responses of these 1×1 structures were collected in a manner described in section 2.1. It is seen that an increase in wavelength results in a stiffer response.

3.1.2. Effect of roughness amplitude

Sinusoidal roughness textures featuring $(a, R_a) = (4 \times 10^{-5}, 23\mu m), (4 \times 10^{-4}, 231\mu m)$, and $(8 \times 10^{-4}, 464\mu m)$ with wavelength $\lambda = 1.076\ mm$ were implemented on lattices. A uniform displacement boundary condition was imposed as described in section 2.1. Stress-strain curves for lattice structures with different surface roughness and various number of repeat units were simulated and compared as seen in Fig. 4a. A nonlinear relation between stress and strain was seen at a compressive strain $\sim 0.8\%$. The stiffness of the structure was found to monotonically decrease as the magnitude of surface roughness R_a increased as seen in Fig. 4b. Similarly, the stiffness also decreased with an increasing number of repeat units in the lattice. However, this effect decays as a larger number of repeat units is added to the lattice.

3.2. Effect of Porosity Defects on Mechanics of Lattices

3.2.1. Effect of Porosity Density on Mechanics of Lattices

A preset number between $n = 0 - 120$ of elliptical porosity defects was implanted in unit lattices featuring a roughness $R_a = 23\mu m$, prior to application of boundary conditions described in section 2.1. The stress at the strain of 1% and the resulting stiffness of lattice structures within the elastic region in terms of porosity are shown in Figs. 5a, 5b, respectively. It is seen that 2.72% porosity defects each in the top and bottom (horizontal) struts decrease the stress at 1% strain by 4 MPa with respect to the reference sample which did not have any defects (this sample had the same surface roughness and was subject to the same boundary condition as rest of the samples described in this section). In comparison, introduction of an additional 2.98% porosity defects in oblique struts resulted in a steep decline in the stress at 1% strain from 98 to 62 MPa. This is because stress on top and bottom horizontal struts are several orders lower than stress on struts and hence, play a minor role in accommodation of load. Hence, introduction of even a small number of porosity defects in oblique struts results in a steep decline in stiffness. However, the rate of increase in depreciation in mechanical response decreased significantly with increase in defect density. Figure 5b shows the effect of pore size on the resulting stiffness. Trends illustrated in the figure generally show that porosity diameter plays only a secondary role, wherein the primary effect of depreciation of stiffness of a lattice structure arises from the defect area fraction.

3.3. Effect of randomness of pores generation

In order to illustrate the impact of pseudo-randomness, 1×1 lattice structures with surface roughness $R_a = 23\mu m$, number of porosity defects $n = 20$, radius range of porosity defects $U(0.05t_{strut}, 0.2t_{strut})$ and aspect ratio $U(0.7, 1)$ were created for numerical deformation simulations. However, the random number seed was changed to various values that are shown in Fig. 6b. In this figure, the x-axis represents seed for the two oblique struts. For instance, 4&10 in Fig. 6b refers to seed value = 4 for strut that was inclining towards the left and seed 10 for strut that was inclining towards the right. This numerical sample 4&10 was set as reference because all pores that generate on struts in previous sections use this seed combination to generate random numbers. Seed number 1 and 2 were set by default for top shell and bottom shell, respectively. Seed in these cases were used to pseudo-randomly generate numbers for position, radius and aspect ratio of elliptical pores.

It is clear that changes to the random number seed can produce significant variation in the mechanical response of lattices. This is evident from the seed number combination 5&7 that results in a force response which is 12.3% greater than the reference. On the other hand, the seed number combination 18&20 results in a reaction force that is 15.7% lower than the reference.

3.4. Effect of strut angle θ

The effect of strut angle θ on stiffness of 1×1 lattice structures is shown in Fig. 6b. Here, the angle θ corresponds to the oblique angle between two adjacent struts in the structure. The stiffness increases with the increasing θ due to transition from bending dominated to uniaxial compression dominated deformation at higher strut angles. For instance, stiffness values of $2.8 \times 10^{10} N/m^2$ and $1.1 \times 10^{10} N/m^2$ were seen in struts featuring in $\theta = 75°$ and $\theta = 48°$, respectively. In addition to this obvious effect, and interesting observation was made from this effort, *viz.* the rate of decline in stiffness with increasing porosity is greater in slender struts featuring higher angle θ. Further,

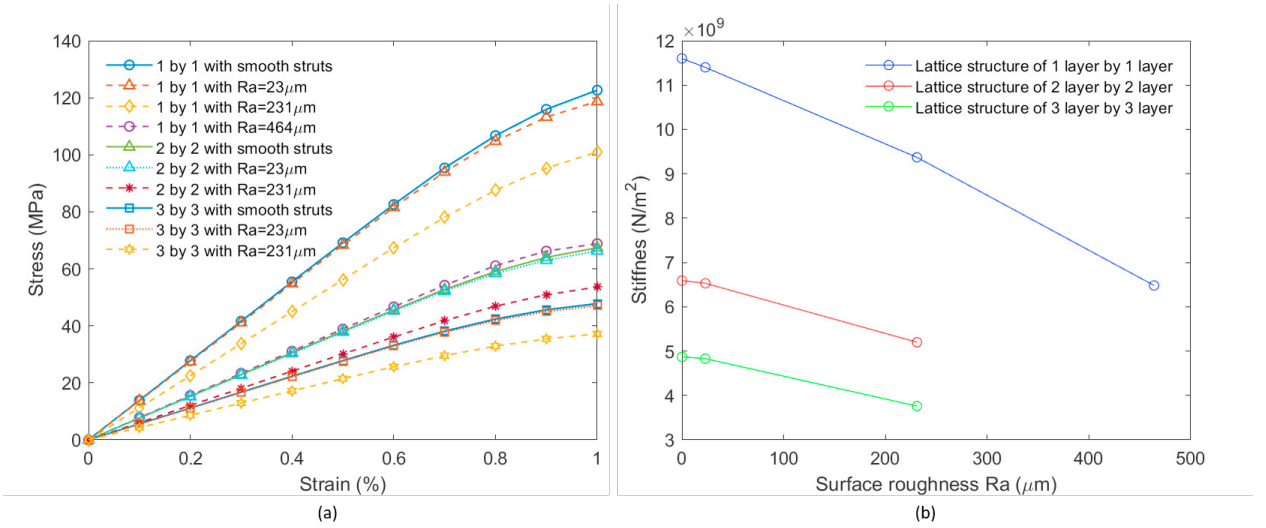

Fig. 4. (a) Stress vs. strain curve for multi-layer lattice structures with different surface roughness; (b) Stiffness vs. Surface roughness Ra. Force is expressed as force per thickness in a plane stress mode, therefore the stiffness discussed in this work is stiffness per thickness in the unit of N/m^2

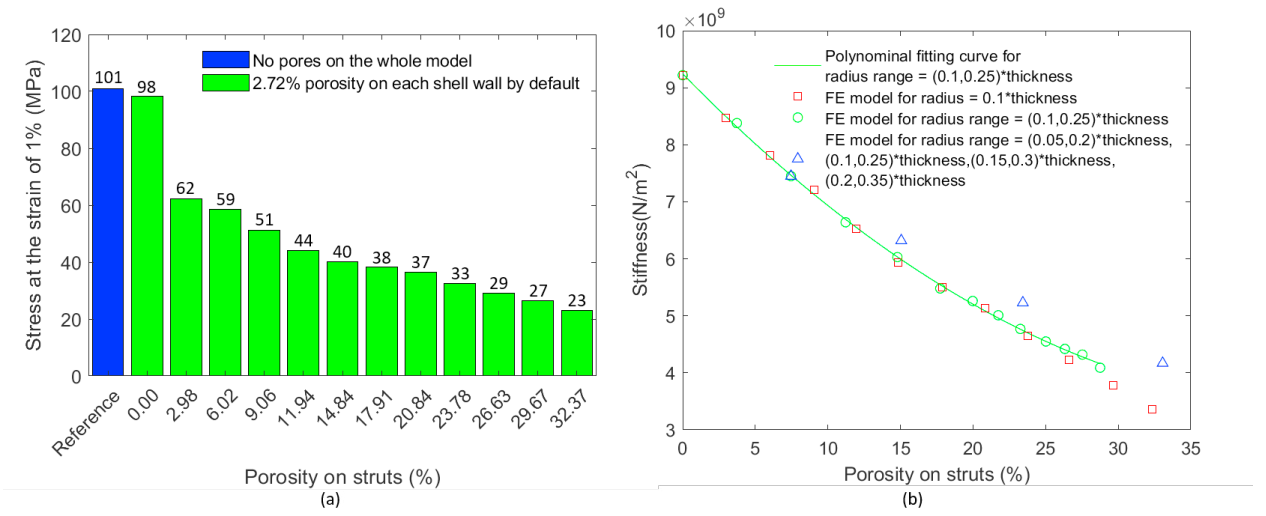

Fig. 5. (a) Effect of number of pores expressed in Stress at the strain of 1% vs porosity; (b) Effect of radius range expressed in Stiffness vs. porosity fitted by a polynominal curve.

the effect of roughness is also more pronounced in larger strut angles θ.

3.5. Implications of this work

The present work creates a workflow that can be used to studying the effect of defects on mechanical response of 2.5D lattice structures. Insights obtained from this work can be used for the following efforts.

1. Establishing a pipeline to produce statistically significant mechanical response data for automating the design of lattice structures.

   Modern advancements in machine learning have enabled frameworks that can accelerate discovery of microstructures. These frameworks rely on training data which is often created using simulations of various combinations of microstructures and loading conditions. Towards this concept, the present work shows an approach to create efficient simulations involving lattice structures. For instance, the present work shows the effect of various res-

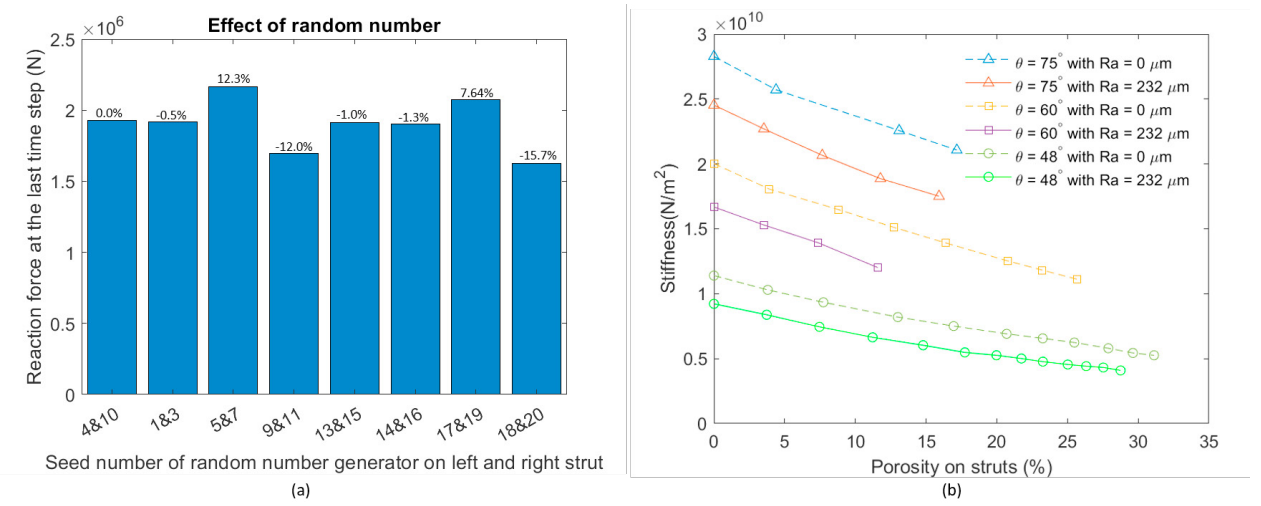

Fig. 6. (a) Effect of random number seeds; (b) Effect of surface roughness on stiffness with different strut angle θ

olutions for discretizing the surface roughness. This effect is tied to the waviness of the surface and is monotonic. This suggests that a coarser resolution may be used to represent roughness in lattice structures and the results can be scaled to generalize insights to a larger domain of defect parameters for saving time during the training phase.

2. Understanding the limitations of computer frameworks for creating stochastic microstructures.

   Section 3.3 provides a discussion of the effects of pseudo-randomness, which exists in many software frameworks. Herein, this work delineates the effect of pseudo-randomness on the mechanical response of lattice structures and suggests that poor combinations of random number seeds may throw the predicted performance off by $>$ 10%. In this regard, this research highlights the importance of optimizing simulations for achieving statistically significant insights on mechanical integrity of structures.

3. Guidelines for designing lattice structures.

   Lattice structures created by additive manufacturing need to be post-processed for making them usable. Post-processing involves rectification of surface and volume porosity defects. Current state of the art technologies cannot be used to rectify all defects that may exist in lattice structures. However, these technologies must create 'good-enough' components. The present work illustrates the dependence of mechanical response of lattice structures, albeit simple, in various defect conditions. In this regard, this framework can be used to make such decisions. In this regard, this framework can be used to optimize the post-processing of lattice structures.

4. Conclusions

The present research utilizes finite element modeling in understanding the effect of roughness and porosity defects on mechanical response of lattice structures. This response was found to be affected adversely by increasing roughness normalized with respect to strut thickness, and porosity size and density. Further, introduction of a small number of defects in load bearing struts was shown to dramatically affect lattice structure's stiffness. It was also seen that the mechanical response of lattice structures is subjective with respect to its defect state. This implies that a combination of different defects can result in the same adverse effect. It was realized that increasing node density on the surface for representation of textures provides diminishing insights. This insight can permit optimization by limiting the required node density to a calibrated threshold value that is governed by the surface texture. Finally, it was seen that algorithms used to implant random defects into microstructures can bias the predicted behavior.

Acknowledgements

This material is based upon work supported by the National Science Foundation under Grant No. 1825686. Any opinions, findings, and conclusions or recommendations expressed in this material are those of the author(s) and do not necessarily reflect the views of the National Science Foundation.

References

[1] Roca, J. B., Vaishnav, P., Fuchs, E. R., & Morgan, M. G. (2016). Policy needed for additive manufacturing. Nature materials, 15(8), 815.
[2] Mukherjee, T., Zuback, J. S., De, A., & DebRoy, T. (2016). Printability of alloys for additive manufacturing. Scientific reports, 6, 19717.
[3] Weißmann, V., Drescher, P., Bader, R., Seitz, H., Hansmann, H., & Laufer, N. (2017). Comparison of single Ti6Al4V struts made using selective laser

melting and electron beam melting subject to part orientation. Metals, 7(3), 91.

[4] Wang, X., Gong, X., & Chou, K. (2017). Review on powder-bed laser additive manufacturing of Inconel 718 parts. Proceedings of the Institution of Mechanical Engineers, Part B: Journal of Engineering Manufacture, 231(11), 1890-1903.

[5] Lewandowski, J. J., & Seifi, M. (2016). Metal additive manufacturing: a review of mechanical properties. Annual review of materials research, 46, 151-186.

[6] Chang, S. H. (2009). In situ TEM observation of γ', γ'' and δ precipitations on Inconel 718 superalloy through HIP treatment. Journal of Alloys and Compounds, 486(1-2), 716-721.

[7] Jia, Q., & Gu, D. (2014). Selective laser melting additive manufacturing of Inconel 718 superalloy parts: Densification, microstructure and properties. Journal of Alloys and Compounds, 585, 713-721.

[8] Deng, D., Moverare, J., Peng, R. L., & Söderberg, H. (2017). Microstructure and anisotropic mechanical properties of EBM manufactured Inconel 718 and effects of post heat treatments. Materials Science and Engineering: A, 693, 151-163.

[9] Trosch, T., Strößner, J., Völkl, R., & Glatzel, U. (2016). Microstructure and mechanical properties of selective laser melted Inconel 718 compared to forging and casting. Materials letters, 164, 428-431.

[10] Mazur, M., Leary, M., Sun, S., Vcelka, M., Shidid, D., & Brandt, M. (2016). Deformation and failure behaviour of Ti-6Al-4V lattice structures manufactured by selective laser melting (SLM). The International Journal of Advanced Manufacturing Technology, 84(5-8), 1391-1411.

[11] Leary, M., Maconachie, T., Sarker, A., Faruque, O., & Brandt, M. (2019). Mechanical and thermal characterisation of AlSi10Mg SLM block support structures. Materials & Design, 183, 108138.

[12] Ptochos, E., & Labeas, G. (2012). Elastic modulus and Poisson's ratio determination of micro-lattice cellular structures by analytical, numerical and homogenisation methods. Journal of Sandwich Structures & Materials, 14(5), 597-626.

[13] Kang, D., Park, S., Son, Y., Yeon, S., Kim, S. H., & Kim, I. (2019). Multi-lattice inner structures for high-strength and light-weight in metal selective laser melting process. Materials & Design, 175, 107786.

[14] Deshpande, V. S., & Fleck, N. A. (2001). Collapse of truss core sandwich beams in 3-point bending. International Journal of Solids and Structures, 38(36-37), 6275-6305.

[15] Queheillalt, D. T., & Wadley, H. N. (2005). Cellular metal lattices with hollow trusses. Acta Materialia, 53(2), 303-313.

[16] Wang, J., Evans, A. G., Dharmasena, K., & Wadley, H. N. G. (2003). On the performance of truss panels with Kagome cores. International Journal of Solids and Structures, 40(25), 6981-6988.

[17] Lee, S., Barthelat, F., Moldovan, N., Espinosa, H. D., & Wadley, H. N. (2006). Deformation rate effects on failure modes of open-cell Al foams and textile cellular materials. International Journal of Solids and Structures, 43(1), 53-73.

[18] Doyoyo, M., & Hu, J. W. (2006). Multi-axial failure of metallic strut-lattice materials composed of short and slender struts. International journal of solids and structures, 43(20), 6115-6139.

[19] Prabhakar, P., Sames, W. J., Dehoff, R., & Babu, S. S. (2015). Computational modeling of residual stress formation during the electron beam melting process for Inconel 718. Additive Manufacturing, 7, 83-91.

[20] Khairallah, S. A., Anderson, A. T., Rubenchik, A., & King, W. E. (2016). Laser powder-bed fusion additive manufacturing: Physics of complex melt flow and formation mechanisms of pores, spatter, and denudation zones. Acta Materialia, 108, 36-45.

[21] Cerardi, A., Caneri, M., Meneghello, R., Concheri, G., & Ricotta, M. (2013). Mechanical characterization of polyamide cellular structures fabricated using selective laser sintering technologies. Materials and Design, 46, 910-915.

[22] Sing, S. L., Wiria, F. E., & Yeong, W. Y. (2018). Selective laser melting of lattice structures: A statistical approach to manufacturability and mechanical behavior. Robotics and Computer-Integrated Manufacturing, 49, 170-180.

[23] Prabhakar, P., Sames, W. J., Dehoff, R., & Babu, S. S. (2015). Computational modeling of residual stress formation during the electron beam melting process for Inconel 718. Additive Manufacturing, 7, 83-91.

[24] Liu, L., Kamm, P., García-Moreno, F., Banhart, J., & Pasini, D. (2017). Elastic and failure response of imperfect three-dimensional metallic lattices: the role of geometric defects induced by Selective Laser Melting. Journal of the Mechanics and Physics of Solids, 107, 160-184.

[25] Ozel, T., Llanos, I., Soriano, J., & Arrazola, P. J. (2011). 3D finite element modelling of chip formation process for machining Inconel 718: comparison of FE software predictions. Machining Science and Technology, 15(1), 21-46.

[26] Torrano, I., Barbero, O., Kortabarria, A., & Arrazola, P. J. (2011). Prediction of residual stresses in turning of Inconel 718 (Vol. 223, pp. 421-430). Trans Tech Publications.

[27] Lu, X., Jia, Z., Lu, Y., Feng, Y., & Liang, S. Y. (2017). Predicting the surface hardness of micro-milled nickel-base superalloy Inconel 718. The International Journal of Advanced Manufacturing Technology, 93(1-4), 1283-1292.

[28] Storey, B. D. (2002). Computing Fourier series and power spectrum with Matlab. TEX paper.

[29] Ås, S. K., Skallerud, B., & Tveiten, B. W. (2008). Surface roughness characterization for fatigue life predictions using finite element analysis. International Journal of Fatigue, 30(12), 2200-2209.

[30] Dallago, M., Winiarski, B., Zanini, F., Carmignato, S. & Benedetti, M., (2019). On the effect of geometrical imperfections and defects on the fatigue strength of cellular lattice structures additively manufactured via Selective Laser Melting. International Journal of Fatigue, 124, 348-360.

[31] Lozanovski, B., Leary, M., Tran, P., Shidid, D., Qian, M., Choong, P. & Brandt, M., (2019). Computational modelling of strut defects in SLM manufactured lattice structures. Materials and Design, 171, p.107671.

[32] Du Plessis, A., Yadroitsava, I., Kouprianoff, D., & Yadroitsev, I., (2018). Numerical and experimental study of the effect of artificial porosity in a lattice structure manufactured by laser based powder bed fusion. Solid Freeform Fabrication 2018: Proceedings of the 29th Annual International, 808-820

[33] Janbaz, S., Bobbert, F. S. L., Mirzaali, M. J., & Zadpoor, A. A., (2019). Ultra-programmable buckling-driven soft cellular mechanisms. Materials Horizons, 6(6), 1138-1147.